Vibrational spectroscopy of cold and water containing molecular ions in a radio frequency ion trap

Steffen Spieler

10. Januar 2018

Contents

Abstract

This report to the Austrian Marshall Plan Foundation summarizes the work conducted in Professor Mark Johnson's lab at the Sterling Chemistry Laboratory at Yale University in New Haven. Goal was to gain deeper insight to the temperature behavior upon cryogenic ion trapping and buffer gas cooling of cationic ammonia-water complex. The hydrated ammonia molecule was generated using conventional electro spray ionization. The ions were transfered by radio frequency ion guides into a cryogenic octupole ion trap at high vacuum conditions. Buffer gas cooling was applied to thermalize the ions with the trap walls which were kept at temperatures in the range of $5\,K$ to $25\,K$. The ions were extracted and flight time separated by means of a reflectron type time of flight mass analyzer. High resolution vibrational dissociation spectroscopy was performed on the asymmetric NH_4^+ stretch mode at different ion trap temperatures. The light source was a injection seeded grating stabilized optic parametric oscillator combined with a optic parametric amplifier which was commisioned and characterized in the scope of this visit. The obtained mid infrared spectra of the cationic ammonia-water complex were compared to rotationally resolved simulations in order to obtain the temperature of the ions depending on the rotational state population. Upon hydration the symmetry group of ammonia, which is of spherical top symmetrie gets changed to be of symmetric top symmetry. The influences of the symmetry group on the nuclear spin statistics was investigated in order to reproduce the rotational state distribution. A significant deviation of the ion temperature from the trap temperature was found. Besides the trap induced heating mechanisms, the influence of rotational constants on collisionally induced rotational cooling is discussed.

Zusammenfassung

Dieser Bericht fasst die Arbeiten und Ergebnisse zusammen, die im Rahmen eines durch die Österreichischen Marshall Plan Stiftung mitfinanzierten Aufenthalts in Professor Mark Johnson's Laboren an der Yale University durchgeführt wurden. Ziel war die Untersuchung der Temperatur des kationischen, kryogen gekühlten Ammonium-Wasser Komplexes. Als Kühlschema wurde Kollisionskühlen mit einem inerten, kalten Puffergas angewendet. Erzeugt wurde der Komplex mittels konventioneller Elektrospray Ionisation. Die Ionen wurden mit radiofrequenz Führungsfeldern in eine kryogen gekühlte Oktupol-Ionenfalle unter Hochvakuumbedingungen geladen. Ein inertes Puffergas wurde zum Kühlen externer und interner Freiheitsgrade der Ionen in die Falle geleitet. Die Fallentemperatur und damit auch die Puffergas Temperatur wurde zwischen $5\,K$ und $25\,K$ variiert. Die Ionen wurden aus der Falle in ein Flugzeit Massenspektrometer geleitet. Hochaufgelöst wurden Vibrationsdissoziationsspektren auf der asymmetrischen NH_4^+ Streckmode bei verschiedenen Temperaturen aufgenommen. Als kohärente Lichtquelle wurde ein pump- und gitterstabilisierter optisch parametrischer Oszillator in Betrieb genommen und verwendet. Die gewonnenen, rotationsaufgelösten Infrarotspektren des kationischen Ammonium-Wasser Komplexes wurden mit temperaturabhängigen Simulationen verglichen. Aufgrund der starken Wechselwirkung des Wassermoleküls mit dem Ammonium ändert sich letzrere Symmetriegruppe von sphärisch symmetrisch zum symmetrischen Kreiselmolekül. Der Einfluss dieser Änderung auf die Kernspinstatistik der jeweiligen Symmetriegruppe wurde untersucht, um die Zustandsbesetzung der Rotationszustände aus dem Experiment zu reproduzieren. Dabei wurde eine signifikante Abweichung der Ionentemperatur von der Fallentemperatur festgestellt. Neben den bekannten Heizmechanismen in Radiofrequenzfallen wird der Einfluss von Rotationskonstanten auf die Effizienz von Kollisionskühlen diskutiert.

1 Introduction

Charge transfer processes of weakly bound ionic systems in the gas phase can be studied using radio frequency ion traps. Hereby a weakly bound system is referred to be a non-covalently bound cluster or complex, mostly held together by means of a hydrogen bond or by van der Waals interaction. However, many atom weakly bound systems possess many degrees of freedom and thereby only stably exist in gas phase at low temperatures and in a non destructive environment, namely where the number density of collisional partners is low. Such an environment is provided inside a multipole radio frequency ion trap. The ability to cool the afore mentioned radio frequency ion trap and the within stored ions to temperatures at which the internal energy of the system is sufficiently below dissociation opens the possibility to study weakly bound systems by spectroscopic and mass spectrometric means. Structural information on these systems can be gained for instance by applying vibrational spectroscopy methods where vibrational transitions allow to deduce the strength of intramolecular bonds and identify binding partners. In combination with quantum chemical calculations, such as density functional theory or ab initio methods, the structure of a molecular system can be deduced.
A simple but versatile method of cooling molecular ions is by thermalizing the trapped ions with a cold gas. Translational and internal degrees of freedom of the ion can be quenched upon elastic or inelastic collisions with a so called cold buffer gas. Typically the ion trap itself is mounted on a helium cryostat and a buffer gas introduced into the trap will thermalize with the trap walls on short time scales. The general assumption in the field of cryogenic radio frequency ion traps was that the ion temperature follows the temperature of the buffer gas which is assumed to be in thermal equilibrium with the cryogenic ion trap walls. However recent studies have found a disagreement with this assumption in the very low temperature range below 30 Kelvin [1]. The question whether the cooling rate upon collisional thermalization of molecular ionic rotations is fundamentally limited, or external heating rates caused by black body radiation and other trapping effects just exceed the cooling rates remains to be answered.
The scope of this report is to summarize the work being conducted to determine the ion temperature by high resolution rotationally resolved vibrational spectroscopy on the free proton bound ammonia-water rotor $NH_4^+ \cdot H_2O$. This system has been used among others to determine the ion temperature by comparing the rotationally resolved spectra with simulated temperature dependent rotationally resolved vibrational spectra. Particular focus here are the symmetry changes upon hydration with one water molecule as well as the nuclear spin statistics. Latter are of importance when investigating temperature dependent transition intensities.

This report is organized as follows: Section 2 gives a general introduction to ion traps and the properties of the trapped ions mostly focusing on the temperature. Section 3 summarizes the methods most commonly used for the production and identification of weakly bound charged systems. The light source commissioned, characterized and used for high resolution spectroscopy is discussed in Section 3.4. Finally, in Section 4 the high resolution spectra of $NH_4^+ \cdot H_2O$ for different temperatures are shown, discussed and compared to simulations. Section 5 summarizes the results and proposes approaches towards a better understanding of the thermal behavior of ions in multipole traps.

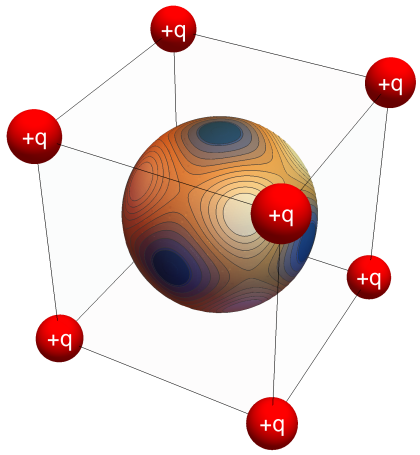

Figure 1: *Earnshaw's theorem: Static arrangement of charges in which a charge q_i cannot be stably trapped. The inner sphere shows the equipotential lines of the potential created by the charges. The blue areas show that the trap is "leaking".*

2 Multipole radio frequency ion traps

The idea of Nobel laureate Wolfgang Paul to apply electric multipolar fields to charged particles in three focusing dimensions led to the invention of multipole ion traps [2]. They not only provide a controlled environment with minimized interactions but enable to mass selectively trap particles and perform spectroscopy on a well focused ion package that can be stored on long time scales. To further reduce the interaction with the electric multipolar field, Dieter Gerlich invented higher order multipolar traps, in particular octupole and 22-pole ion traps [3].
In the following, the basic multipole ion trap concepts for multipole order $n > 2$ will be summarized as well as the versatile technique of buffer gas cooling and ion temperature determination.

2.1 Basic principles

The fact that a charge q experiences a force F when exposed to another charge Q is quantified by the Coulomb interaction

$$\mathbf{F}_{qQ} = \frac{1}{4\pi\epsilon_0}\frac{qQ}{|\mathbf{r}_q - \mathbf{r}_Q|^3}(\mathbf{r}_q - \mathbf{r}_Q).$$

The sign of the force, namely if it is attractive or repulsive, depends on the sign of the charges. In a naive picture one could think that stably trapping a charged particle q_i in three dimensions should be possible when statically arranging charges around q_i. Hereby the sign of neither the charge to be trapped nor the confining static charges should play a role, because all forces cancel out each other (see Figure 1). However when analyzing the potential Φ

$$\mathbf{F}_{qQ} = -\nabla\Phi$$

of static charges in the center of the arrangement, one can only find a saddle point which does not permit stable trapping. The fact that this electrostatic trap is "leaking" or in other words that

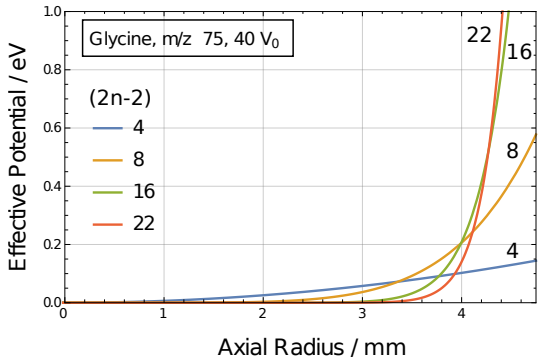

Figure 2: *Effective potential from Equation 1 for glycine (m/z 75) as function of distance to the trap center for different multipole ion traps.*

electrostatic fields cannot confine a charge stably is called the Earnshaw theorem.
However, time dependent electric fields in a linear arrangement can create a field minimum in the center. The spacial and time dependent potential in cylindrical coordinates is given by

$$V(r,\phi,t) = V_0 \cdot cos(n\phi)\left(\frac{r}{R_0}\right)^n sin(\omega t),$$

where $\omega = 2\pi f$ is the angular radio frequency with amplitude V_0, n the multipole order and R_0 the inscribed radius of the confining electrodes [4]. The motion of a charge in a potential with multipole order $n \leq 2$ can be described by the effective potential

$$V_{eff}(r) = \frac{1}{4m}\left(\frac{qnV_0}{\omega R_0}\right)^2\left(\frac{r}{R_0}\right)^{(2n-2)}. \quad (1)$$

Figure 2 shows the effective potential for protonated glycine (m/z 75) as function of radial distance to the trap center axis. In color different multipole trap types, namely quadrupole (4), octupole (8), hexadecapole (16) and twenty two pole (22). The higher the multipole order n, the less the ion dynamics inside the trap is perturbed by the radio frequency.
The effective potential depth of the multipole trap is on the order of a few hundred meV. In the case of glycine this still corresponds to velocities of $700\,m/s$. For precise ion-neutral reaction rate measurements, Doppler free spectroscopy or formation of van der Waals complexes the ions have to be translationally cooled. For ions where no laser cooling schemes are available, the most simple method is by introducing elastic and inelastic collisions with a neutral cold buffer gas. Therefor the ion trap is mounted on a cryostat which allows for tunable temperatures of the trap in the range of typically $300 - 3\,K$.
The buffer gas introduced into the trap is thermalized with the cold trap walls. The time $t_e = (n_{bg} \cdot k)^{-1}$ needed to thermalize the ions with the cold buffer gas depends on the buffer gas density n_{bg} and the Langevin collision rate coefficient

$$k = \frac{|q|}{2\epsilon_0}\sqrt{\frac{\alpha}{\mu}},$$

where α denotes the neutral buffer gas polarizability and μ the reduced mass [4]. t_e typically lies in the range of milliseconds thermalization time until a Maxwell-Boltzmann distribution of the kinetic energies at a given temperature is reached [4].

2.2 Ion temperature determination

The knowledge and control of the ion temperature with sufficient accuracy is not only essential for reaction and collision rate measurements in ion traps, but also for vibrational and rotational spectroscopy, where the temperature T_{ion} of the complex determines its internal energy

$$E_{vib} = (3N - 6) \cdot k_B T_{ion}, \tag{2}$$

here in the case of a non-linear N-atomic molecular system. A temperature hereby is defined as the intensive property of a microcanonical ensemble in thermodynamical equilibrium described by a Maxwell-Boltzmann distribution of the populated rotational states.
The most accurate molecular ion temperatures of buffer gas thermalized systems where no laser cooling schemes are available are based on a rotational state J dependent photodetachment scheme on anionic hydroxyle OH^- [5]. The idea behind this method is to measure the photodetachment rate

$$n_{PD} \propto \sum_{j,J} \sigma_{PD}(j \leftarrow J) \cdot p(T, J).$$

Latter depends on the photodetachment cross section σ_{PD} following a Wigner threshold law behavior and the temperature dependent rotational state population $p(T, J)$. The rotational state specific population $p(T, J)$ can be determined by fitting the measured photodetachment rate which allows to directly determine the internal ion temperature T_{ion}. For $T_{ion} \leq 20\,K$ only the $J = 0$ and $J = 1$ rotational state are significantly populated.
This scheme to determine the ion temperature of collisionally cooled ions has been applied to OH^- by several groups [5, 6, 7]. It was found that the ions internal temperature T_{ion} can be collisionally cooled down to $T_{ion} \sim 15\,K$. Colder internal temperatures by collisional cooling have not been reported although the storage device temperatures and thereby assuming the buffer gas temperatures are significantly below $15\,K$. The same phenomenon was reported by [8, 9, 10] when looking at rovibrational transitions or hot bands of cationic systems.
A different experimental approach to determine the ion temperature was rotational state dependent photo dissociation of CH^+ using a ultra high vacuum cryogenic electrostatic storage ring. No active cooling scheme was applied. The storage time of the ions was chosen to be much longer than the excited rotational state life times (typically on the order of $0.1\,s$ to $100\,s$). However, the ion temperature was limited by black body radiation and the deduced temperature found to be approximately $20\,K$ [23].
A third way of cooling internal degrees of freedom is evaporatively. The (internal) energy of a cluster is reduced by evaporation until the cluster temperature is below the binding energy of the weakest bound cluster atom/molecule.

Several heating mechanisms are under discussion [1, 11]. Radio frequency induced heating of the ion ensemble is known to be relevant for ion traps of low multipole order. Furthermore, a large buffer gas to ion mass ratio, too high endcap potentials, rod misalignment, an overloaded trap, black body radiation, incomplete buffer gas thermalization and hot neutral gas collision can causes an increase in ion temperature. However, most of these parameters can be well controlled and the reasons for the inability to collisionally cooling rotational degrees of freedom of trapped ions below $15\,K$ are still not entirely clear.

3 Cold ion vibrational predissociation

The invention of the electrospray ionization method by Noble laureate John Fenn provides an interface between liquid phase chemistry and gas phase spectrometry. The combination of afore mentioned methods has not only provided deep insight to structural properties of chemically and biologically relevant systems but evolved to a billion dollar market in the field of analytical chemistry. Ion guides, filters, traps and mass analyzers of various types are combined to study sample composition, reactions and dissociation behavior on a high level accuracy. Fundamental structural information and dynamics can be gained by combining upper ion manipulation methods with electronic, vibrational and rotational spectroscopy.
This chapter is attributed to briefly introduce the experimental methods, namely elecrospray ionization, time of flight mass spectrometry, the cold ion trap setup and the narrow band optic parametric oscillator (OPO) and optic parametric amplifier (OPA) system.

3.1 Electrospray ionization

Gasphase studies on molecular ions that possess one or a combination of the following properties, namely being thermally fragile, possessing high molecular weight and low polarity are prime target species of electrospray ionization. The target species typically is solvated in $mMol/l$ to $uMol/l$ concentrations in a water, methanol or acetonitrile solution. Solvated basic molecules form cations due to proton transfer from acids formed in autoprotolysis of the solvent. Solvated acidic molecules form anions. The level of protonation or deprotonation can be enhanced by adding an acid or a base, respectively. The solution containing the ion is pressed through a needle at ambient pressures. A voltage between the liquid and a capillary into the vacuum vessel is applied. Due to the interaction of the charges in the solution with the electric field on the one hand and surface tension of the solution on the other hand, a Taylor cone forms at the tip of the needle. Latter bursts into droplets when the charge repulsion inside the jet overcomes the surface tension (Rayleigh limit). The droplets containing the target ions further undergo fission and solvent evaporation. The remaining ions are transfered in a laminar flow through the capillary into the vacuum apparatus.

3.2 Time of flight mass spectrometry

Besides the afore mentioned quadrupole radio frequency ion guides, mass selection and separation can be achieved by time of flight mass spectrometry. In a repulsive potential difference U an ion of charge $q = ze$ converts its potential energy

$$E_{pot} = ze \cdot U = \frac{1}{2} m v^2 = E_{kin}$$

into kinetic energy. After traveling a fixed distance s the arrival time t of the ion is

$$t = a \cdot \sqrt{\frac{m}{z}},$$

where $a = s^2(2eU)^{-1} = const$. Elaborate techniques such as Wiley-McLaren dual stage acceleration for velocity and spacial spread compensation of the initial ion beam as well as kinetic energy

spread compensation by reflectron mirrors enhance the mass resolution R of time of flight mass separators.

$$R = \frac{m}{\Delta m} = \frac{t}{2\Delta t}$$

The resolution is a measure how well masses are separated in time or space after traveling a defined distance or time, respectively.

3.3 Experimental setup

A schematic drawing of the setup used for the current experiments can be found in [12] with the only difference of possessing an octupole ion trap instead of a Paul trap. Briefly, the source region is a conventional electrospray source including a syringe pump, a fused silica capillary, a $30\,\mu m$ needle and a $0.5\,mm$ transfer capillary. The design and dimensions of the transfer region namely capillary length and vacuum pressures in the first vacuum chamber are crucial for the production of water clusters. The ions are guided by means of octupole ion guides through four differentially pumped stages to a region of $\sim 10^{-7}\,mbar$, before loaded into a cryogenic octupole ion trap. In this pressure region, the mean free path of an ion is on the order of $\sim km$, providing a background collision free, well controlled environment. The trap temperature can be set in a range of $300 - 4.5\,K$. A dense helium buffer gas pulse created by a solenoid valve can be injected directly into the trap. For two main reasons helium is chosen as an ideal buffer gas. First, it is inert, meaning no chemical reactions occur upon collision with the trapped ions and second, it remains in gas phase even at temperatures down to $4\,K$. The ions are stored and thermalized with the cold buffer gas for $65\,ms$ before being ejected into a Wiley-McLaren accelerator. Several meters downstream the mass separated ions are spatially focused into the laser interaction region before passing a mass gate, a reflectron mirror and finally a MCP detector. The whole experiment runs on a $10\,Hz$ repetition rate. The voltage drop on the MCP caused by hitting ions is recorded by a digital oscilloscope. The traces of parent ions as well as laser fragments can be integrated for typically 4 experimental cycles. The integrated fragment signal is plotted as function of current OPO wavelength. For low resolution scans, the scanning speed of the OPO was set to $3\,cm^{-1}/s$. Typically 4 scans always from the red to the blue were taken. The OPO output power is constantly locked and can be used later on for power normalization of the spectrum.

3.4 Grating stabilized seeded OPO/OPA

A schematic drawing of the commercial optic parametric oscillator and amplifier system (Laser Vision) is shown in Figure 3, upper panel. The system is pumped by $1064\,nm$, $\leq 600\,mJ/pulse$, flash lamp pumped Nd:Yag laser operated at $10\,Hz$. The pump laser can be injection seeded by a narrow band diode laser. A fraction of the pump beam gets frequency doubled ($532\,nm$) and fed into an OPO (KTP crystal). Parametric conversion splits the incident pump photon of frequency ν_p into one signal ν_s (near IR) and one idler ν_i photon (mid IR), a three-photon process which obeys energy conservation $\nu_p = \nu_s + \nu_i$ and momentum conservation $\vec{p_p} = \vec{p_s} + \vec{p_i}$. Latter allows for a wide tunability of the frequency of the outgoing photons by rotation of the non-linear crystal. The signal of the OPO stage gets fed into a $1064\,nm$ pumped optic parametric amplifier dual stage (KTA crystal).

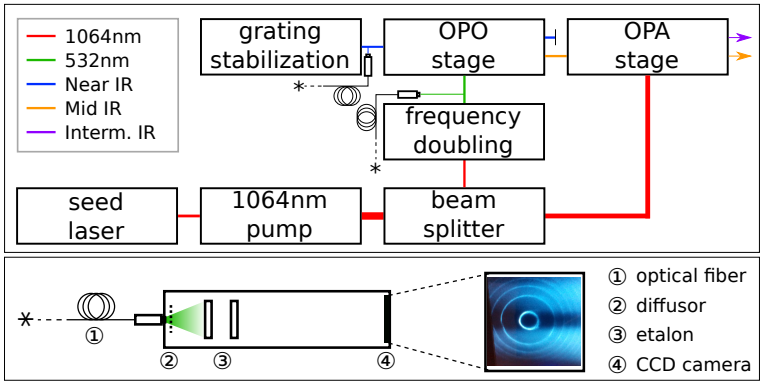

Figure 3: *Upper panel (modified from Laser Vision user manual): Schematic diagram of the OPO/OPA system including fiber coupling of the monitored pump and near IR wavelength. Lower panel: Fiber coupled etalon assembly. The interference pattern was monitored by a CCD camera giving crisp rings for single mode operation.*

The typical line width of the free running system is $\sim 4\,cm^{-1}$ while with injection seeded (single mode) pump laser $\sim 2\,cm^{-1}$ was reached. The output power at $500\,mJ/p$ pump power and $3400\,cm^{-1}$ was $\sim 17\,mJ/p$. To further narrow the line width down, the signal of the OPO stage hits a tunable grating. The narrow band first order of the reflection is coupled back into the cavity and forces the OPO to run in single mode operation. The line width of the outgoing mid IR beam reaches $0.1\,cm^{-1}$ or lower, at a nominal output power of $\sim 5\,mJ/p$ at $580\,mJ/p$ pump power and $3400\,cm^{-1}$.
In order to guarantee a mode hop free tuning and proper seeding of the OPO/OPA system, both the interference pattern of the injection seeded, frequency doubled pump laser was monitored as well as the near IR signal of the grating stabilized OPO stage. Therefore the light of each individual stage was fiber coupled and diffusely fed into two Fabry-Pérot interferometers (etalon crystals). The interference pattern of the incident light with itself was monitored by a CCD camera. Unseeded operation allows for many transverse modes of slightly different wavelength within the gain profile of the medium. Fed into an etalon, the interference pattern gives broad or even no rings. However, when properly seeded, the laser/OPO is forced to run in single mode operation, giving crisp interference rings. This ring structure is conserved, although the diameter D of the k^{th} ring changes by $D = \sqrt{b \cdot k\lambda + 1}$ continuously when the wavelength λ of the laser is scanned[1].

To characterize the OPO/OPA system's performance, vibrational transmission spectroscopy was performed on a gas cell containing the neutral spherical top molecule methane (CH_4) at a pressure of $\sim 0.5\,mbar$ to minimize pressure broadening. The OPO/OPA power transmitted through the cell was recorded by a bolometer as function of wavelength. The summarized results are shown in Figure 4 (i)-(vi). Figure 4 (i) shows a full broadband scan of the vibrational transitions of CH_4 at $296\,K$ overlayed by a stick spectrum taken from the HITRAN on web database. Figure 4 (ii) compares a scan of the unseeded (blue) with the injection seeded (orange) pump laser. The unseeded FWHM line width of the vibrational transitions was determined to be $3.5\,cm^{-1}$ while the injection seeded transitions showed a line width of $2.2\,cm^{-1}$. Figure 4 (iii) shows a scan with grating stabilized, injection seeded OPO/OPA. The background structure shows a minimum

[1] $b = 8s^2/2d$, s distance etalon-screen, d etalon thickness

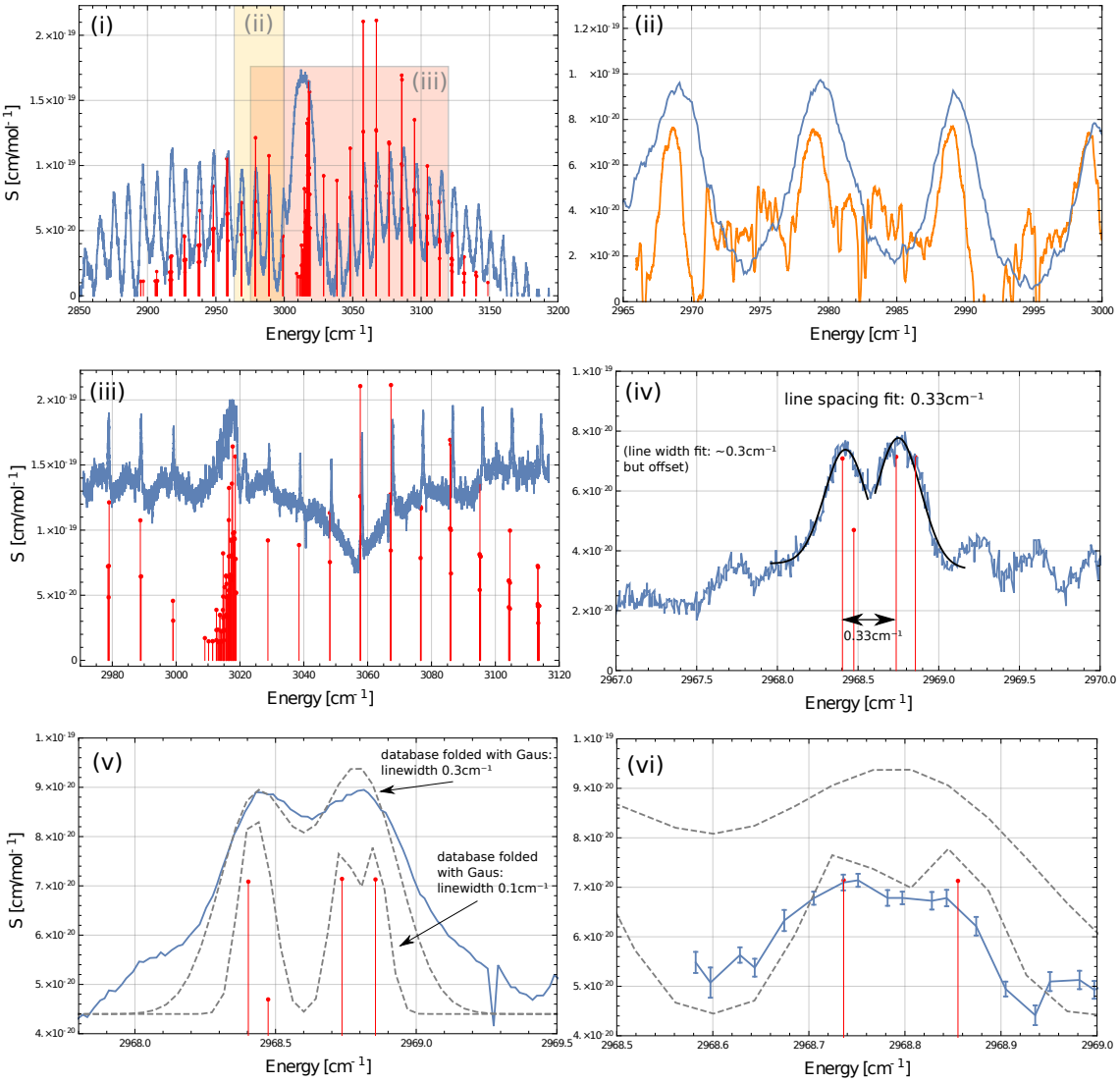

Figure 4: *(i) Broadband scan (blue) over P-, Q- and R-branch of neutral CH_4. In red the stick spectrum for CH_4 at 296 K taken from the HITRAN on web database. (ii) Broadband scan (blue) versus injection seeded (orange) in a narrow range. (iii) Injection seeded, grating stabilized scan (blue). (iv) Zoom into (iii). (v) Comparison of different line width for a 12 times averaged narrow band spectrum (blue). (vi) 25 averages step scan of two asymmetric vibrational stretch transitions separated by 0.12 cm^{-1}*

at $\sim 3055\,cm^{-1}$ which is due to increasing laser power. Figure 4 (iv) shows a zoom and two normal distribution fits yielding a FWHM line width of $0.3\,cm^{-1}$. The high resolution scans were taken at a scanning speed of $0.1\,cm^{-1}/s$. Figure 4 (v) shows a 12 fold averaged spectrum over a more narrow region of (iv). The dashed curves are folded normal distributions of line width $0.3\,cm^{-1}$ and $0.1\,cm^{-1}$, respectively, centered around the asymmetric vibrational stretch transitions of different rotational states. Figure 4 (vi) shows a scan, where the system was parked for $90\,s$, while the power on the bolometer was averaged before moving to the next frequency at steps of $0.025\,cm^{-1}$.
In conclusion, the injection seeded grating stabilized narrow band OPO/OPA system was commissioned. The neutral gas spectroscopy states a line width of $\sim 0.3\,cm^{-1}$ in scanning mode. The resolution might be improved by slower scanning or stepping.

3.5 OPO frequency calibration

In order to provide spectra with reliable photon energies, a recalibration of the OPO system has to be carried out on a regular basis. However, the time between recalibrations depends on the aimed absolute accuracy and the stability of the OPO/laser system. Typically when investigating vibrational transitions of cryogenically cooled ions without resolving rotational features, the observed linewidth is given by the OPO linewidth which is typically in the range of several wavenumbers. The stability of the motors that rotate the crystals is good enough to recalibrate on the timescale of several months. In order to recalibrate the system the signal wavelength is measured by a wavelength meter and compared to the wavelength given from the parameter set of the OPO at given motor positions. A wavelength meter typically is a combination of several Fizeau type interferometers. The interference pattern is read out by a CCD and the pattern is compared to a data base in order to obtain a wavelength. Mechanical stress and temperature fluctuations can affect the absolute accuracy. Therefore the wavelength meter it self has to be calibrated. This can be done, either like in the present study by comparing to a neutral gas transmission spectroscopy. The transitions of HCl, NH_3, CH_4, H_2O among many others, can be used depending on the energy range of interest. The rotationally resolved vibrational transitions of these species are known to a very high level of absolute accuracy. Another way is to calibrate the wavelength meter by using calibration lasers such as temperature stabilized helium-neon lasers, (frequency doubled) Nd:Yag lasers or lasers locked to atomic transitions such as cross-over resonances in rubidium or cavity locked lasers. Again, the stability of the wavelength meter determines how often recalibrations of the measuring device it self have to be carried out.
It is important to note that recalibrations of both the OPO system as well as the wavelength meter have to be carried out on a regular basis in order to provide reliable absolute photon energies.

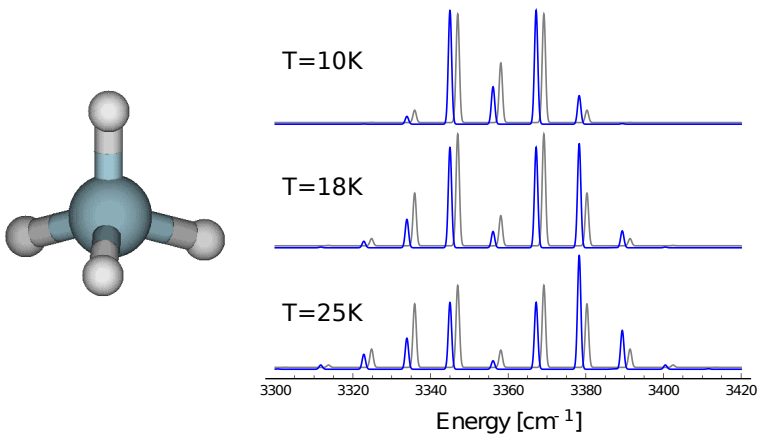

Figure 5: *Structure and simulated rovibrational spectrum for $T = 10, 18, 25\,K$ of NH_4^+. In gray the unscaled and in blue the according to the nuclear spin statistical weights scaled transitions. The unscaled spectrum is offsetted in intensity and in energy by $2\,cm^{-1}$ for better visibility of the effect. The line width of the transition was set to $1\,cm^{-1}$*

4 Temperature determination of $NH_4^+ \cdot H_2O$

The (ion) temperature describes the translational energy distribution of an microcanonical ensemble of ions by a Maxwell-Boltzmann distribution. According to the equipartition theorem, the thermal energy is equally distributed over all external and internal degrees of freedom. Thereby knowledge of the population of rotational states of a molecular ensemble allows to determine its temperature. Quantum mechanical effects such as Fermi-Statistics for identical spin 1/2 particles have to be taken into account when determining temperatures based on state populations.
The following chapter is attributed to determine the molecular symmetry group of the bare and hydrated ammonium molecule in order to assess the importance of nuclear spin statistical effects on the state population. In both cases the theoretical rotational spectrum is investigated and compared to rotationally resolved vibrational dissociation measurements. The temperature of the ensemble is deduced by simulating the transition intensities with two independent programs (pgopher and asyrotWin), which refers to the temperature dependent state populations.

4.1 Ammonium and water: Symmetry considerations

In an aqueous solution, ammonia forms the ammonium cation and the hydroxyle anion

$$NH_3 + H_2O \rightleftharpoons NH_4^+ + OH^-.$$

The ammonium cation is a spherical top molecule of tetrahedral symmetry and thereby in the $T_d(M)$ point group. All three moments of inertia $I_a = I_b = I_c$ are equal, giving the vibrational ground state rotational energy of the system in a specific rotational state J to be

$$E_{rot}^{v_0}(J) = B_0 J(J+1) - D_0 J^2(J+1)^2 + D_T f(J,\kappa), \tag{3}$$

where B_0 is the vibrational state dependent rotional constant and D_0 the centrifugal distortion. The third term is a product of the quartic tensor centrifugal distortion constant D_T which in Oka's

experiments was determined to be $4.8 \cdot 10^{-6}\, cm^{-1}$ with the tetrahedral splitting $f(J, \kappa)$ [13]. (For a molecule of T_d symmetry, $f(J = 6, \kappa = F_1) < 2000$ making the third term neglectable for low J values [14]). For the vibrationally excited molecule, the rotational energy is given by

$$E_{rot}^{v_3}(J) = \nu_0 + B_3 J(J+1) - 2B_3\zeta_3 \mathbf{J} \cdot \mathbf{L} - D_s \mathbf{J}^4 + \ldots,$$

however fine structure is neglected here.
The molecule possesses $(3 \cdot 5 - 6) = 9$ vibrational modes. Due to the spherical symmetry, the symmetric stretch vibration (ν_1) and the two-fold degenerate symmetric bend (ν_2) are dipole forbidden. The asymmetric stretch vibration ν_3 as well as the asymmetric bend are both three-fold degenerate and IR active. The vibrational ground state rotational constant B_0 as well as the v_3 rotational constant B_3 were determined by Oka [13] and can be taken from Table A.1. The population of rotational levels of a spherical top molecule

$$f(J, T) = \frac{(2J+1)^2 \cdot exp\left(-\frac{E_{rot}(J)}{k_B \cdot T}\right)}{\sum_J (2J+1)^2 \cdot exp\left(-\frac{E_{rot}(J)}{k_B \cdot T}\right)} \tag{4}$$

depends on the temperature T. However, due to two pairs of identical nuclei with spin $I_i = 1/2$ with $i = 1 - 4$ the population of each rotational state is affected and hence the transition probabilities. Bunker and Jensen [15] tabulated the nuclear spin statistical weights of each representation in the T_d point group, namely $A_1, A_2 = 5$, $E = 2$ and $F_1, F_2 = 3$. They also tabulated the symmetry species for each rotational state, summarized until $J = 6$ in Table A.2. It can be seen, that from $J = 2$ on the rotational states split into different transitions, if the molecule is vibrating. Using Equ. 3, 4 and the statistical weights, the rovibrational spectrum of NH_4^+ at $T = 10$, 18, $25\, K$ were calculated for unscaled (gray) and scaled (blue) transitions (see Figure 5). As rotational constant $B = B_0 + B_3 - 2B_3\zeta_3$ was used. ζ_3 is the coriolis coupling constant and accounts for changes in the rotational velocity, and thereby the rotational constant, upon molecular vibrational contraction due to angular momentum conservation. In contrast to [9] it is worth noting that even at low temperatures the nuclear spin statistics significantly changes the rotational spectrum.

Upon hydration, the proton bound system of water and ammonium

$$NH_4^+ \cdot H_2O$$

is of $G_{12} = C_{3v} \times C_s$ extended molecular symmetry group. Due to the hydrogen bonding, the weakly bound molecule is considered to be a free internal rotor with vanishing interaction between the water and the ammonium group and thereby can be treated by its individual point groups. However, due to the long-range charge-dipole interaction of the NH_4^+ upon hydrogen bonding to the water molecule, the point group of the ammonium changes to be C_{3v} of a symmetric top molecule.

4.2 Rotationally resolved vibrational spectroscopy

Ammonium water was produced by electro spraying a basic solution ($pH = 8$) of NH_4OH in water. The weakly bound systems were trapped for $65\, ms$ in an octupole ion trap. The temperature of the trap was tuned in the range of 5 to $25\, K$. Thereby the internal energy of the molecule was

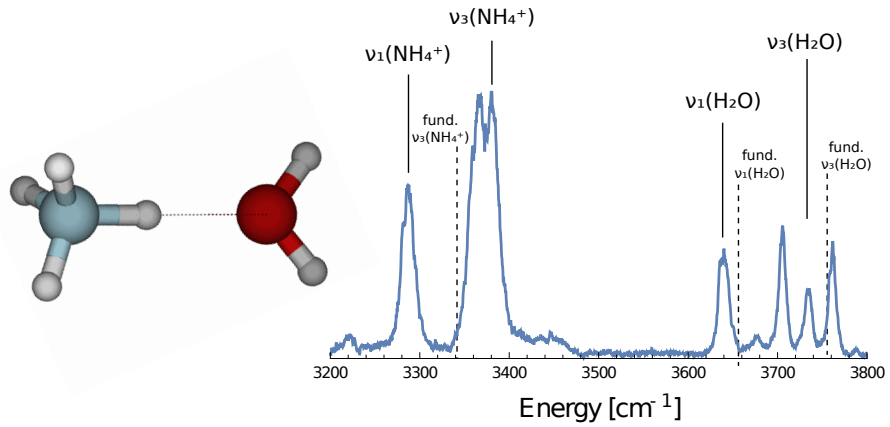

Figure 6: *Experimental NH_4^+ signal growth of the $NH_4^+ \cdot H_2O$ parent system at 4 K as function of OPO/OPA photon energy. Data provided by Stephanie Craig.*

63 to 313 cm^{-1}. In an action spectroscopy scheme, the weakly bound system dissociates upon resonant vibrational excitation if the energy of the excited vibrational mode exceeds the binding energy of the system. The calculated dissociation energy of $NH_4^+ \cdot H_2O$ is $\sim 6200\,cm^{-1}$ [16], so two resonant photons are required. Distributing the energy of the first photon of $3300\,cm^{-1}$ over the $(3 \cdot N - 6)$ vibrational modes of the system heats it up to a temperature of $\sim 264\,K$ before the second photon drives the dissociation.

The molecular structure of the two intermolecular rotors and a broadband overview scan taken at 4 K by Stephanie Craig is shown in Figure 6. The symmetric $\nu_1(NH_4^+)$ vibrational transition in contrast to the bare cation is IR active upon polarization by the water molecule and centered around $3285\,cm^{-1}$. This vibrational anisotropy causes the $\nu_3(T2)$ band of NH_4^+ to split into a parallel (A1) and a perpendicular (T2) transition of a symmetric top molecule. The symmetric water stretch $\nu_1(H_2O)$ is centered around $3640\,cm^{-1}$. In both cases, the asymmetric stretch is rotationally resolved with its center at $3380\,cm^{-1}$ and $3735\,cm^{-1}$ for the ammonium and water, respectively. While the symmetric and asymmetric water stretches are red shifted by $14\,cm^{-1}$ and $20\,cm^{-1}$, the asymmetric NH_4^+ stretch is blue shifted by $38\,cm^{-1}$, showing nicely the cooperativity/anticooperativity effect[2]. Dopfer et al. found a blue shift of $1\,cm^{-1}$ for the system $NH_4^+ \cdot He$ and concluded the ammonium to be almost unperturbed remaining in T_d symmetry [17], while Bieske et al. found a much stronger intermolecular anisotropic interaction in the rotational-vibrational spectrum of $NH_4^+ \cdot Ar$ [18]. The vibrational anisotropy V_2 of $NH_4^+ \cdot H_2O$ is $95\,cm^{-1}$ and thereby $3\,cm^{-1}$ larger than in the case of $NH_4^+ \cdot Ar$ measured by Bieske.

Due to the larger rotational constant of water ($B = 14.5\,cm^{-1}$) the rotational spacing for the water system is larger than for ammonium ($B = 5.9\,cm^{-1}$). To resolve the rotational lines of the NH_4^+ moiety, the injection seeded grating stabilized OPO/OPA introduced in Section 3.4 was used. Figure 7 shows the high resolution spectra of the NH_4^+ asymmetric stretch transition at three different temperatures. A number of $\Delta K = \pm 1$ Q branches, separated by $\sim 11\,cm^{-1}$ are visible which is in fair agreement with the bare NH_4^+ rotational constant. Some of the K subband Q branches

[2]Gorlova, Johnson, to be published

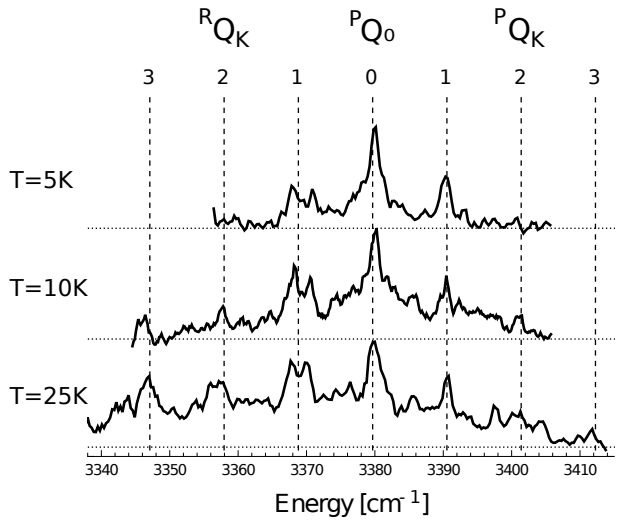

Figure 7: *High resolution spectrum of the $\nu_3(NH_4^+)$ transition for three different trap temperatures $T = 5,\ 10,\ 25\,K$. The different K subbands of the Q-branches show an increase in population with increasing temperature.*

split into two lines which was also seen by Bieske in the case of $NH_4^+ \cdot Ar$. The interpretation of this splitting was "a tunneling splitting of substantially hindered internal rotation, between four equivalent positions, of the NH_4^+ unit within the $Ar - NH_4^+$ complex" [18]. The tunneling effect increases with ion temperature, which can be seen by the increase of unresolved features in between the Q branches. To estimate the rotational anisotropy, the intermolecular potential has to be simulated. Besides the study of vibration-rotation tunneling interactions of charged spherical top molecules upon binding with rare gas atoms, Saykally and coworkers investigated neutral van der Waals bound complexes of water and hydrophobic molecules [19] and found similar effects.

Figure 8 (a) finally shows a temperature simulation for a symmetric top molecule for a pure perpendicular transition. The simulation was done with asyrotWin [20]. The rotational constants for both, the lower vibrational state and the excited state were obtained by DFT methods using Gaussian (freq=vibrot) by [21] and are given in Table A.1. The band origin was set to $3380\,cm^{-1}$, the number of unique nuclear spin isomers was set to 2. The correlation of Cartesian coordinates to principal axes was set to III^r convention. The assumed linewidth was $1\,cm^{-1}$.
The temperature of the octupole ion trap was $T = 10\,K$. Although taking nuclear spin statistics into account, the transition intensities and the line splitting are not quite reproduced by the simulation. Figure 8 (b) takes the mixture of the transition dipole moment into a perpendicular and parallel transition into account . Concerning the temperature of the ions a rough estimate can be made, however including large uncertainties. The common trend of incomplete ion thermalization can be seen, since the $10\,K$ simulation is not in agreement with the data when looking at the red Q branches. Furthermore a slight overestimation of the rotational constants can be seen. Figure 8 bottom shows pgopher simulations [22] of a A1 type transition with slightly adapted rotational ground state and excited state constants. The nuclear spin statistics are taken into account, the simulated temperatures were $10\,K$ (c) and $40\,K$ (d). The assumed Gaussian linewidth was $0.5\,cm^{-1}$. According to the pgopher simulation the spectrum agrees best with an ion temperature of $40\,K$

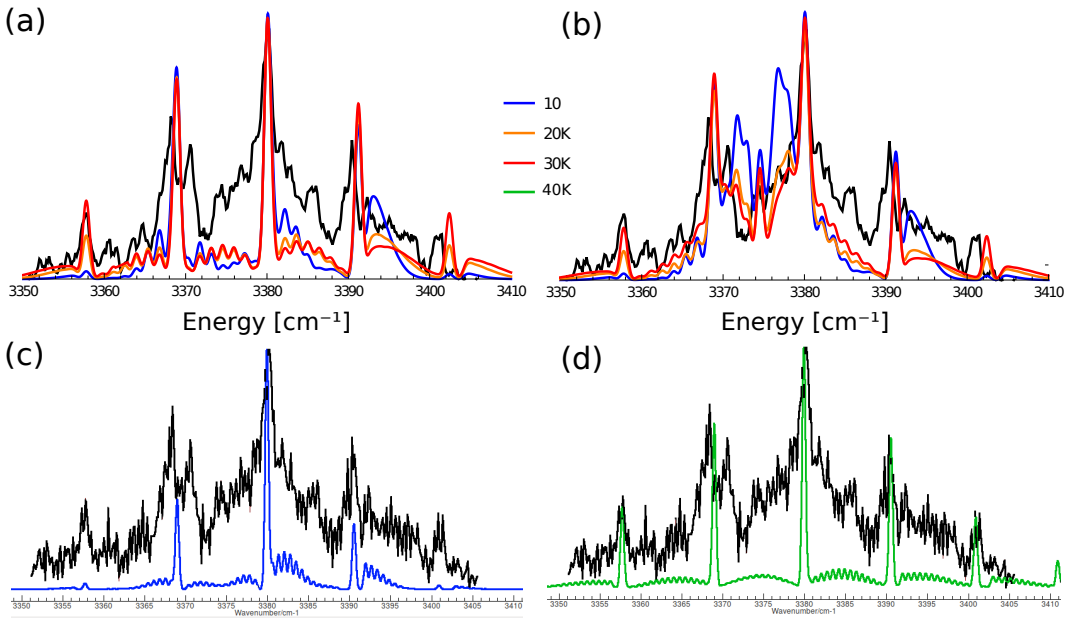

Figure 8: *Temperature simulation for temperatures of* 10, 20, 30 , 40 *K (blue, orange, red, green, respectively). The data (black) was taken at* 10 *K trap temperature. (a) asyrotWin simulation for a pure A1 perpendicular transition. (b) asyrotWin for perpendicular and parallel transition. pgopher simulation with slightly adopted rotational constants for (c)* 10 *K of a A1 type transition and (d)* 40 *K.*

which is a factor of 4 off the trap temperature.

4.3 Cooling of internal energy

The internal rotational energy partition function for a spherical rotor with rotational constant B is given by

$$Z = \sum_{J=0}^{J_{max}} (2J+1)^2 \cdot exp\left(-\frac{B}{k_B \cdot T} \cdot J(J+1)\right).$$

Two regimes can be distinguished, the classical regime where $T \gg B$ and the quantum regime $T \ll B$. In the classical regime the quantization of rotational states is irrelevant. In the quantum regime the temperature is much smaller than the rotational constant, meaning that the spacing $2B$ between the rotational ground state and first excited rotational state is large compared to the temperature, rotational degrees of freedom are frozen out.
In the case of ammonium the spacing between the rotational ground state and the first excited state corresponds to $15.8\,K$ ($= 2B = 11\,cm^{-1}$) while the ensembles temperature was determined in a range below $15\,K$. For OH^- $2B = 2 \cdot 19.12\,cm^{-1} = 55.0\,K$ rendering an extreme case for the decoupling of internal degrees of freedom to external ones.
It is known that collisional cooling rates using monoatomic buffer gas depend on the energy level spacing. Larger spacing leads to more inefficient cooling, which was demonstrated by Duncan in the case of a symmetric top molecule with efficient collisional cooling of small J spaced levels compared to inefficient cooling of largely spaced K rotational levels [24, 25].

5 Conclusion

Gas phase ion vibrational spectroscopy using cryogenic ion traps provides a well controllable environment to study fundamental structural and kinetic properties of charged species. Although mulitpole ion traps are designed for minimized perturbation of the ion's motion inside the trap by radio frequency electric fields, some mechanisms permit the complete cooling of the internal and external degrees of freedom of the ions. This conclusion can be drawn by summarizing the findings of several groups working with both cations and anions applying different trapping and cooling techniques such as radio frequency multipole ion traps combined with buffer gas cooling or electrostatic storage rings and rotational state down cascading by trapping longer than the exited rotational state lifetimes [23]. The first experimental finding of the ions internal rotational temperature in agreement with the temperature of the cryogenic environment achieved by improved shielding of black body radiation field was reported by [6]. For most experiments simulating ionic destruction and formation processes in the interstellar medium or obtaining vibrational ground state properties of complex systems, temperatures on the order of $10\,K$ are sufficiently cold. However, the origin of the inability to cool rotational degrees of freedom of complex molecules below $10\,K$ remains unclear.
In the present study temperature dependent rotationally resolved spectra of the symmetric top molecule $NH_4^+ \cdot H_2O$ were compared to simulations of the rotational state population. The knowledge of the nuclear spin statistics of the molecule is crucial for calculating the rotational state distribution. However, due to the strong vibrational anisotropy of the system, the molecular symmetry group is not obvious. The interaction of the water with the ammonium is too strong to treat latter as an unperturbed spherical top. Furthermore the coupling between the charged NH_4^+ moiety and the water make a free rotor model questionable. Additional vibration-rotation tunneling splittings enhance the complexity of the spectrum. In conclusion, the system might not be the best choice for accurate temperature determination.
Anyways, the simulations suggest a ion temperature of $20 - 40\,K$ while the cryogenic ion trap was kept at $10\,K$. In the present experiment the most probable heating mechanism might be collisional heating due to an overfilled ion trap. Heating due to high end cap voltages or RF amplitudes is considered unlikely in the present study. The end cap voltages were $< 2\,V$ above trap float and the RF amplitudes were $< 10\,V_{pp}$. It might be worth trying a depletion measurement looking at mass m/z 36 with a low number of trapped ions instead of a enhancement measurement at m/z 18 with saturated parent signal. In line with the collisional heating mechanism, a reduction of the cycle time of the experiment might be worth testing to allow for better pumping of the buffer gas before ion extraction. To avoid the additional difficulty of the complexity of ammonium-water, the well established OH^- photodetachment could be tried by using the signal of the OPO system as photodetachment laser around $680\,nm$ to determine the octupole ion trap performance upon translational and internal cooling.
Furthermore it has to be kept in mind that the equipartition theorem (see Section 4) breaks down, if the temperature of the ion ensemble is smaller than the level spacing between ground and first excited rotational state. This rises the question if the term temperature is meaningful when dealing with molecular ionic ensembles at temperatures below $10\,K$ and rotational constants on the order of $10\,cm^{-1}$.

System	B_0/cm^{-1}	D_0/cm^{-1}	B_3/cm^{-1}	ζ_3/cm^{-1}	source
$T_d(NH_4^+)$	5.92932	$-1.282 \cdot 10^{-4}$	5.8764	0.06038	[13]
$C_{3v}(NH_4^+)$	$A = 5.9293$, $B = C = 0.35482$		$A = 5.9355$, $B = C = 0.35482$		[21]

Table A.1: *Rotational constants, centrifugal distortion and coriolis coupling taken from [13].*

J	Γ_{rot}	weight
0	A_1	5
1	F_1	3
2	$E + F_1$	5
3	$A_2 + F_1 + F_2$	11
4	$A_1 + E + F_1 + F_2$	13
5	$E + 2F_1 + F_2$	11
6	$A_1 + A_2 + E + F_1 + 2F_2$	21

Table A.2: *Rotational state dependent symmetry and nuclear spin statistical weights for T_d point group, taken and extended from [15].*

6 Appendix

References

[1] Endres, E. S., Egger, G., Lee, S., Lakhmanskaya, O., Simpson, M., and Wester, R. (2017). Incomplete rotational cooling in a 22-pole ion trap. Journal of Molecular Spectroscopy, 332, 134-138.

[2] Paul, W. (1990). Electromagnetic traps for charged and neutral particles (Nobel lecture). Angewandte Chemie International Edition, 29(7), 739-748.

[3] Gerlich, D. (1992). Inhomogeneous rf fields: a versatile tool for the study of processes with slow ions. State-selected and state-to-state ion-molecule reaction dynamics. Part, 1, 1-176.

[4] Wester, R. (2009). Radiofrequency multipole traps: tools for spectroscopy and dynamics of cold molecular ions. Journal of Physics B: Atomic, Molecular and Optical Physics, 42(15), 154001.

[5] Otto, R., von Zastrow, A., Best, T., and Wester, R. (2013). Internal state thermometry of cold trapped molecular anions. Physical Chemistry Chemical Physics, 15(2), 612-618.

[6] Schmidt, H. T., Eklund, G., Chartkunchand, K. C., Anderson, E. K., Kamińska, M., de Ruette, N., ... and Rosén, S. (2017). Rotationally Cold OH Ions in the Cryogenic Electrostatic Ion-Beam Storage Ring DESIREE. Physical Review Letters, 119(7), 073001.

[7] Meyer, C., Becker, A., Blaum, K., Breitenfeldt, C., George, S., Göck, J., ... and Herwig, P. (2017). Radiative rotational lifetimes and state-resolved relative detachment cross sections from photodetachment thermometry of molecular anions in a cryogenic storage ring. Physical Review Letters, 119(2), 023202.

[8] Rizzo, T. R., Stearns, J. A., and Boyarkin, O. V. (2009). Spectroscopic studies of cold, gas-phase biomolecular ions. International Reviews in Physical Chemistry, 28(3), 481-515.

[9] Kelleher, P. J., Johnson, C. J., Fournier, J. A., Johnson, M. A., and McCoy, A. B. (2015). Persistence of Dual Free Internal Rotation in NH4+ (H2O)· He n= 0–3 Ion–Molecule Complexes: Expanding the Case for Quantum Delocalization in He Tagging. The Journal of Physical Chemistry A, 119(18), 4170-4176.

[10] Heine, N., and Asmis, K. R. (2015). Cryogenic ion trap vibrational spectroscopy of hydrogen-bonded clusters relevant to atmospheric chemistry. International Reviews in Physical Chemistry, 34(1), 1-34.

[11] Asvany, O., and Schlemmer, S. (2009). Numerical simulations of kinetic ion temperature in a cryogenic linear multipole trap. International Journal of Mass Spectrometry, 279(2), 147-155.

[12] Wolk, A. B., Leavitt, C. M., Garand, E., and Johnson, M. A. (2013). Cryogenic ion chemistry and spectroscopy. Accounts of chemical research, 47(1), 202-210.

[13] Crofton, M. W., and Oka, T. (1987). Observation of forbidden transitions of ammonium ion (NH+ 4) 3 band and determination of ground state rotational constants. Observation of 3 band allowed transitions of ND+ 4. The Journal of chemical physics, 86(11), 5983-5988.

[14] Kirschner, S. M., and Watson, J. K. (1973). Sextic centrifugal distortion of tetrahedral molecules. Journal of Molecular Spectroscopy, 47(2), 347-350.

[15] Bunker, P. R., and Jensen, P. (1999). Spherical top molecules and the molecular symmetry group. Molecular Physics, 97(1-2), 255-264.

[16] Pankewitz, T., Lagutschenkov, A., Niedner-Schatteburg, G., Xantheas, S. S., and Lee, Y. T. (2007). Infrared spectrum of NH 4+(H 2 O): Evidence for mode specific fragmentation. The Journal of chemical physics, 126(7), 074307.

[17] Dopfer, O., Nizkorodov, S. A., Meuwly, M., Bieske, E. J., and Maier, J. P. (1996). The 3 infrared spectrum of the He NH4+ complex. Chemical physics letters, 260(5-6), 545-550.

[18] Bieske, E. J., Nizkorodov, S. A., Dopfer, O., Maier, J. P., Stickland, R. J., Cotterell, B. J., and Howard, B. J. (1996). Observation of the infrared spectrum of the 3 band of the argon-ammonium ionic complex. Chemical physics letters, 250(3-4), 266-272.

[19] Dore, L., Cohen, R. C., Schmuttenmaer, C. A., Busarow, K. L., Elrod, M. J., Loeser, J. G., and Saykally, R. J. (1994). Far infrared vibrationrotationtunneling spectroscopy and internal dynamics of methane–water: A prototypical hydrophobic system. The Journal of chemical physics, 100(2), 863-876.

[20] Judge, R. H., and Clouthier, D. J. (2001). AsyrotWin: A 32-bit Windows version of Asyrot, A program for the analysis of high resolution singlet-singlet band spectra of asymmetric tops. Computer physics communications, 135(3), 293-311.

[21] Huang, Meng, Washington State University, private communication.

[22] Western, C. M. (2010). PGOPHER, a program for simulating rotational structure. University of Bristol, 7, 108.

[23] O'Connor, A. P., Becker, A., Blaum, K., Breitenfeldt, C., George, S., Göck, J., ... and Hechtfischer, U. (2016). Photodissociation of an Internally Cold Beam of CH+ Ions in a Cryogenic Storage Ring. Physical review letters, 116(11), 113002.

[24] Scurlock, C. T., Pullins, S. H., Reddic, J. E., and Duncan, M. A. (1996). Photodissociation spectroscopy of Ca+–H2O and Ca+–D2O. The Journal of chemical physics, 104(12), 4591-4599.

[25] Vaden, T. D., Lisy, J. M., Carnegie, P. D., Pillai, E. D., and Duncan, M. A. (2006). Infrared spectroscopy of the Li+(H 2 O) Ar complex: the role of internal energy and its dependence on ion preparation. Physical Chemistry Chemical Physics, 8(26), 3078-3082.